Energy & Buildings 282 (2023) 112792

Contents lists available at ScienceDirect

Energy & Buildings

journal homepage: www.elsevier.com/locate/enb

Modelling and optimization of domestic thermal energy storage based heat pump system for geothermal district heating

Oguz Arslan [a,*], Asli Ergenekon Arslan [b], Taqiy Eddine Boukelia [c]

[a] Mechanical Engineering Department, Engineering Faculty, Bilecik Seyh Edebali University, Bilecik, Turkey
[b] Quality Control in Manufacturing Programme, Vocational School, Bilecik Seyh Edebali University, Bilecik, Turkey
[c] Mechanical Engineering Department, Jijel University, Jijel, Algeria

ARTICLE INFO

Article history:
Received 30 October 2022
Revised 19 December 2022
Accepted 8 January 2023
Available online 10 January 2023

Keywords:
Efficiency analysis
Exergy analysis
District heating
Geothermal heat pump
Thermal energy storage

ABSTRACT

In this study, a new residential heat pump system was designed for domestic use in the geothermal district heating system (GDHS). A heat pump system was integrated into the substations of the residences with this aim. The heat pump system was formed by replacing the conventional evaporator with thermal energy storage (TES) unit. In this regard, a shell and tube latent heat TES system was used and designed for the peak loads. 66 different systems were parametrically formed and analyzed thermodynamically. The observed cases were later evaluated from economical and environmental points of view. Finally, the most appropriate system was determined by a multi-criteria decision-making analysis named efficiency analysis technique with output satisficing (EATWOS). It was concluded that it is available to obtain an investable design with an NPV value of 6.35 million $, exergy efficiency of 15.24% and CO_2 reduction of 1435.32 ktons per year.

1. Introduction

Depending on the environmental issues and experienced global crisis of fossil fuel, renewable energy sources came into prominence in recent years. The effective and efficient use of these renewable sources has a key role in this regard. Geothermal energy is the most stable one amongst the renewable since it has no fluctuating from the time and physical properties points of view. However, the geothermal resources are limited depending on the reservoirs' capacity. So, geothermal energy systems still need to be improved for a sustainable future.

Geothermal energy is used for many purposes such as balneological use, power generation, refrigeration and heating of spaces [1–3]. District heating systems are the most common one of the utilizing methods of geothermal sources [4,5]. In a common geothermal district heating system (GDHS), the heat of the geothermal fluid is transferred to a secondary fluid through a main heat exchanger system as the first step. Later, this heat is transferred to heating circuit systems through a substation heat exchanger system to be used for the final heating purposes of the buildings. These kinds of systems are designed for peak loads according to the meteorological conditions of the districts. These systems work constantly under these conditions although there is no need for peak requirements [6,7]. Thus, these kinds of systems need to be improved to avoid this wasting energy and overconsumption of electricity as well as to increase efficiency.

Thermal energy storage (TES) based district heating systems (DHS) are an alternative solution in this sense [8]. Knudsen et al. [9], in their study, indicated that it is possible to achieve a 12 % reduction of effective peak heating with TES use in DHS sourced by industrial waste heat. Zhang et al. [10] investigated the applicability of TES in the low-temperature DHS. They indicated that the central tank is the most favourable for variable renewable energy. they also indicated that the benefits of the TES in small-scale systems can not offset the increased network heat losses since the storage capacity is less than 1 % of the daily load. Saloux and Candanedo [11] indicated it is available to obtain an annual saving of 47 % on pump electricity use by the seasonal TES-integrated DHS sourced by solar energy. Li et al. [12], in their study, indicated that it is possible to achieve a 5 % annual saving of reduction of effective peak-heating with a TES use in DHS sourced by the waste heat of data centres. Arslan and Arslan [13], in their study, indicated that it is possible to achieve an electricity-saving of 30.24 GWh and a heat-saving of 130.94 GWh per year through the TES integrated DHS sourced by geothermal energy. TES-integrated DHS are also effective systems from the environmental, economic, and efficiency points of view. Rezaie et al. [14], in their study, indicated

* Corresponding author.
E-mail address: oguz.arslan@bilecik.edu.tr (O. Arslan).

https://doi.org/10.1016/j.enbuild.2023.112792
0378-7788/

Nomenclature

A	area (m2)
C	cost ($)
Cp	Specific heat (kJ/kgK)
D	diameter (m)
E	multi-criteria efficiency
$\dot{E}$	energy rate (kW)
$\dot{E}x$	exergy rate (kW)
F	enforced convection boiling factor or correction factor
G	mass velocity
Gr	Grashof number
h	convective heat transfer coefficient (W/m2K) or specific enthalpy (kJ/kg)
ip	distance matrices for input (kg/m2s)
J	dimensionless heat factor
k	conductive heat transfer coefficient (W/mK)
$\dot{m}$	mass flow rate (kg/s)
n	number of plates or pipe
Nu	Nusselt number
op	distance matrices for output
P	pressure (kPa. bar. or atm)
Pr	Prandtl number
$\dot{q}$	heat rate per length (kW/m)
$\dot{Q}$	heat rate (kW)
r	radius (m) or normalized output
Re	Reynolds number
s	specific entropy (kW/kgK) or normalized input
S	effectiveness factor
T	temperature (K or oC)
U	Total heat transfer coefficient (W/m2K)
v	weight for output
V	volume (m3)
w	weight for input
$\dot{W}$	work rate (kW)
x	input value, dryness fraction
X	input matrices
Xt	Martinelli parameter
y	output value
Y	output matrices

Greek symbols

β	volumetric expansion coefficient (-)
ε	exergy efficiency (%)
H	energy efficiency (%)
Λ	friction factor
μ	dynamic viscosity (Ns/m2)
N	Specific volume (m3/kg)
P	density (kg/m3)
σ	surface tension (N/m)
ψ	specific flow exergy (kJ/kg)

Subscripts

b	boiling
d	destruction
e	enforced convective, electricity saving
f	fluid phase, heat saving
fg	fluid-gas mixture phase
g	gas phase
h	hydraulic
i	inner, inlet or ith component
if	two-phase condition
ins	insulation
k	kth component
lm	logarithmic mean
o	outer, outlet
o&m	Operating and maintenance
T	value at a specified temperature
w	wall conditions
0	value at the reference state

Superscripts

*	normalized values

Abbreviations

C	Heat centre
COP	Coefficient of performance
DHS	District heating system
GDHS	Geothermal district heating system
GWP	Global warming potential
HC	Heating circuit
H-line	Heating zone transmission line
HP	Heat pump
MCDM	Multi-criteria decision making
NPV	Net present value
ODP	Ozone depletion potential
PCM	Phase change material
TbHP	Thermal energy storage-based heat pump
T-line	Geothermal zone transmission line
TES	Thermal energy storage

that it is available to achieve an energy efficiency of 60 % and exergy efficiency of 19 % through the TES-integrated DHS sourced by solar energy. Dorotić et al. [15], in their study, showed that it is available to increase energy efficiency by up to 65 % via the integration of the TES system into DHS sourced by the waste heat, electrical energy, and solar energy. He et al. [16], in their study, determined that it is available to reduce CO_2 emissions by 5480.6 $kgCO_2eq$ per year with a payback period of 3.7 years. Matuszewska et al. [17] also indicated that the mobile TES system is quite effective in the reduction of CO_2 emissions and profitable in distances around 3–4 km. Kyriakis and Younger [18] determined that TES integrated DHS sourced geothermal energy enhances geothermal energy utilization. They also indicated that the two-tank TES system is beneficial depending on the decreased heating cost and emissions.

The integration of heat pump (HP) systems into DHS is also an effective solution for the effective use of energy sources. Arat and Arslan [19,20], in their studies, indicated that it is available to achieve an efficiency value of 76.92 % for the HP-integrated DHS. In the study, a large-scale HP was integrated into the heat centre of DHS with a higher performance coefficient (COP) of 9.56 and a net present value (NPV) of 23,195,962 US$. Wang and Zhang [21] investigated the integration of HP into DHS. They conducted that it is available to increase the heating capacity by 0.4 times in comparison to the conventional system. Zhang et al. [22] conducted a new DHS integrated with ground source absorption HP. They indicated that it is possible to increase the efficiency by 22 % with a decrease of 15 % in heat loads. Marx et al. [23] investigated the integration of HPs into solar district heating (SDH) systems. They concluded that it is available to save primary energy and reduce CO_2 emissions by 69.9 %. Kang et al. [24] investigated the integra-

tion of HP into combined heat and power generation systems. They indicated that the energy efficiency of the new system is 3.9 % higher than the reference system. Bach et al. [25], in their study, investigated the two integration ways of HP into DHS. They conducted that the integration into the distribution network is more attractive than the integration into the transmission network. The highest COP value of the proposed system was recorded at about 3. In the study, it was also suggested that it would be better to operate the HP system at a constant temperature.

From this point, the combined use of TES and HP in DHS can be handled as a better solution. Kim et al. [26], in their study, integrated the TES system with the geothermal heat pump system (GHPS). They indicated that it is available to reduce the operational cost by 36–54 %. Hemmatabady et al. [27], in their study, integrated an HP system into borehole TES-based DHS. In the study, HP was used to boost the stored geothermal energy. They conducted it is available to achieve a decrease in the emission factor by 60 %. Siddiqui et al. [28], in their study, investigated the HP system integrated into a TES-based DHS. They conducted that electricity costs substantially depend on the TES size. They also conducted that the minimum electricity cost was achieved at a TES size of 1 %. Fiorentini et al. [29] investigated the integration of HP and TES into solar DHS. In the study, the heating demand was met by two HP systems namely air-sourced and borehole TES-sourced. They indicated that it is available to reduce CO_2 emissions by up to 43.7 % with a small increase in the annual cost by 6.1 %. Bordignon et al. [30] investigated a TES-based HP system sourced from the waste of a photovoltaic thermal system to be used in DHS. In the study, the highest COP value of the proposed system was recorded as 5.4. In the study, it was also indicated that electricity saving of up to 21 % is available. The studies in the literature show that TES-based HP systems used in DHSs have some advantages from the viewpoints of efficiency, emission reduction and economics. In the large-scale DHS, the required TES size and HP capacity would increase. This issue could cause extra efforts and extra investment costs in the construction phase as well as the operating case. The geographical layout is also another criterion to be taken into account. In this regard, the domestic TES-based HP systems can be an issue for GHDSs. With such a system, it is also possible to achieve higher COP values depending on the thermophysical properties of the geothermal sources.

In this study, a new geothermal district heating system was designed and optimized by multi-criteria decision making for Simav geothermal field. The novelty of this study lies in the integration of residential scale heat pump system into geothermal district heating system. The other crucial novelty lies in the design of heat pump system in which a TES system is used as the evaporator. A domestic shell and tube type TES system including simultaneous charging and discharging by the heating and cooling pipes was integrated with an HP system for the residences for this purpose. A total of 66 different designs were formed by taking the different temperature scales into account. The formed cases were then analyzed by energy and exergy methods. The designs were also investigated from the points of economics and environmental effects. Finally, the most effective design was determined by the multi-criteria decision-making analysis taking the economic, efficiency and environmental issues into consideration.

2. Material and method

The Simav geothermal resources were evaluated in the TES-based HP-integrated GDHS (TbHP-GDHS). Simav geothermal wells with a mass flow rate of 462.0 kg/s and a temperature of 133.5 °C currently heat 5000 residences [7]. In this study, the S-GDHS was planned to heat 12,500 residences. The flow diagram of the TbHP-GDHS is given in Fig. 1.

TbHP-GDHS is formed of five subcomponents namely the geothermal transmission line with the pre-insulated pipes with a 4250 m length (*T*-line), heat centre (C), heating zone transmission line with the pre-insulated pipes with a 4000 m length (H-line), TES based HP substation (HP), and heating circuit (HC). In the study, it was considered that the geothermal water is transported to C after the primary use such as electricity generation throughout *T*-line (points 1–2). The heat of geothermal water is transferred to network water throughout C (points 2–3) via plate-type heat exchangers (HE-1). The heated network water is transported to HP by H-line (points 4–5 and 8–9 for return). Later, the heat of network water is transferred to substations of the buildings via a TES system (points 5–8). TES system is a shell-and-tube-type heat exchanger as seen in Fig. 2. The tube side is formed of two kinds of pipes namely heating and cooling pipes; therefore, it is available to operate simultaneously for both charging and discharging. The shell side is formed of the main structure filled by phase change material (PCM), insulation layer and aluminium cover. The heat transferred from the H-line fluid is stored via heating pipes (points a-d) to feed the vapour compression HP system. The boosted energy by HP is later transferred to the water of HC (points b-c) via a conventional shell-and-tube-type heat exchanger (HE-2). Finally, this heat is transferred to the residences (points 6–7) by the aluminium panel radiators (HE-3) with a height of 600 mm.

According to the related standards [31], the peak heat demand of residences ($\dot{Q}_{design}$) at the design point was 56,130 kW, which means approximately 4.5 kW for each residence [13]. The dynamic heat demand was calculated by taking the meteorological data of the Simav region into account as given in Fig. 3.

According to Fig. 3, the average soil temperature ranges between 5.8 °C and 20.2 °C. The daily average environmental temperature ($T_{outdoor}$) changes between −3.5 °C and 14.9 °C. According to this, the heat demand of the residences ($\dot{Q}_{demand}$) ranges between 20,675 kW and 44,936 kW with heating days of 209 [13].

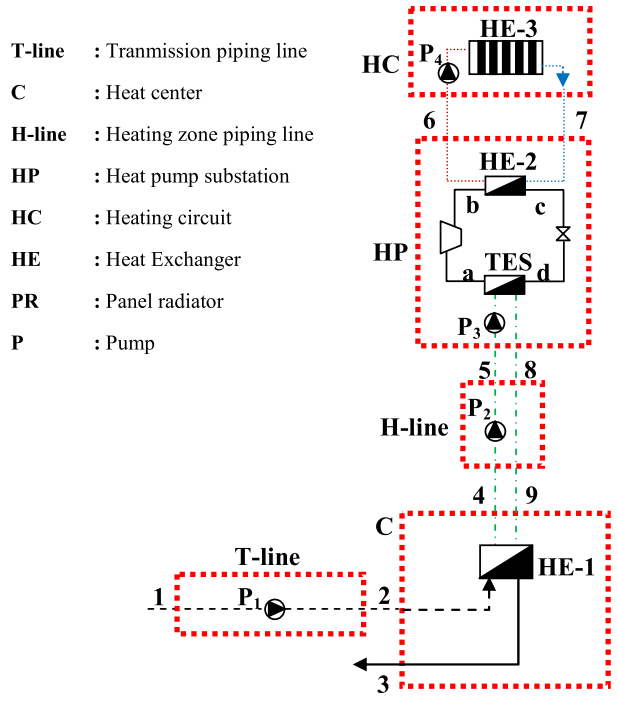

Fig. 1. Flow diagram of TbHP-GDHS.

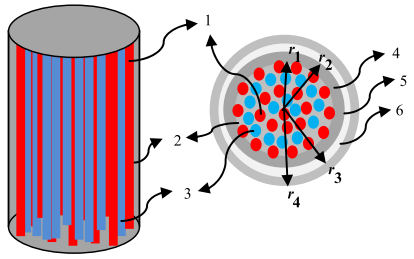

Component	Explanation	Material	Diameter (mm)	Thickness (mm)	k (W/mK)
1	Heating pipe	St37	25	4	170
2	-	PCM	-	-	0.2
3	Cooling pipe	St37	25	4	170
4	Shell	St37	Design parameter	3	170
5	Insulation	Rock wool	-	100	0.035
6	Cover	Al (Embossed)	Design parameter	1	237

Fig. 2. The structure of TES system.

The working fluid for the HP system was chosen considering the available working and environmental conditions such as temperature, ozone depletion potential (ODP) and global warming potential (GWP). Therefore, the working fluid was chosen as R600a since it is commonly used in refrigeration systems in Turkey. The PCM was chosen considering the heat capacity, melting temperature, thermal stability, corrosion effects, lower cost, and higher thermal conductivity. The properties of R600a and PCMs are given in Table 1.

2.1. Modelling of TES-based HP (TbHP) system

In the TbHP system, the TES unit is the evaporator which behaves as a heat source for the HP system. In the system, the heat of the network (water in H-line) is stored by PCM via the heating pipes (marked with "1" in Fig. 1). The length of a single pipe was chosen as 1.5 m with a diameter (D) of 0.025 m and a wall thickness of 0.004 m. The material of the pipes was chosen St37 considering the higher heat conduction coefficient (k_{pipe} = 170 W/mK) and the lower cost. The heat transfer rate of the charging case for a single pipe is given by:

$$\dot{Q}_{pipe,charging} = \overbrace{\frac{1}{\frac{1}{\frac{Nu_i \cdot k_i}{D}} + \frac{r_i}{k_{pipe}} ln\left(\frac{r_o}{r_i}\right) + \frac{r_o}{r_i}\frac{1}{\frac{Nu_o \cdot k_o}{D}}}}^{U_{pipe}} A_{pipe}\left(\left(\frac{T_5 + T_8}{2}\right) - T_{PCM,melting}\right) \quad (1)$$

where r_i, r_o, A_{pipe}, $T_{PCM,melting}$ indicate the inner radius of the pipe, the outer radius of the pipe, the heat transfer area and the melting temperature of PCM. k_i and k_o are the conductive heat transfer coefficients of water and PCM, respectively. Nu_i and Nu_o are the dimensionless heat transfer coefficients (Nusselt number) for the water and PCM, respectively. Since the flow is laminar according to the calculated mass ratios of requirements, *the* Nu_i number of waterside for constant wall temperature is taken as 3.66 [36]. Under natural convection conditions, the Nu number for the PCM side is given by [37]:

$$Nu_o = \frac{0.35 \cdot (Gr \cdot Pr)^{0.25}}{\left(1 - \left(\frac{0.143}{Pr}\right)^{\frac{9}{16}}\right)^{\frac{4}{9}}} \quad (2)$$

where Gr and Pr are the Grashof and Prandtl numbers, respectively. So, the required number of pipes is given as:

$$n_{pipe,charging} = \frac{\dot{Q}_{design}}{\dot{Q}_{pipe,charging}} \quad (3)$$

The stored energy by PCM is later used for the evaporation of the working fluid (R600a) of the HP system. This discharging process is performed by the cooling pipes in a similar way to the charging case. The heat transfer rate of discharging case for a single pipe is given by:

$$\dot{Q}_{pipe,discharging} = \overbrace{\frac{1}{\frac{1}{h_i} + \frac{r_i}{k_{pipe}} ln\left(\frac{r_o}{r_i}\right) + \frac{r_o}{r_i}\frac{1}{\frac{Nu_o \cdot k_o}{D}}}}^{U_{pipe}} A_{pipe}\left(T_{PCM,melting} - \left(\frac{T_a + T_d}{2}\right)\right) \quad (4)$$

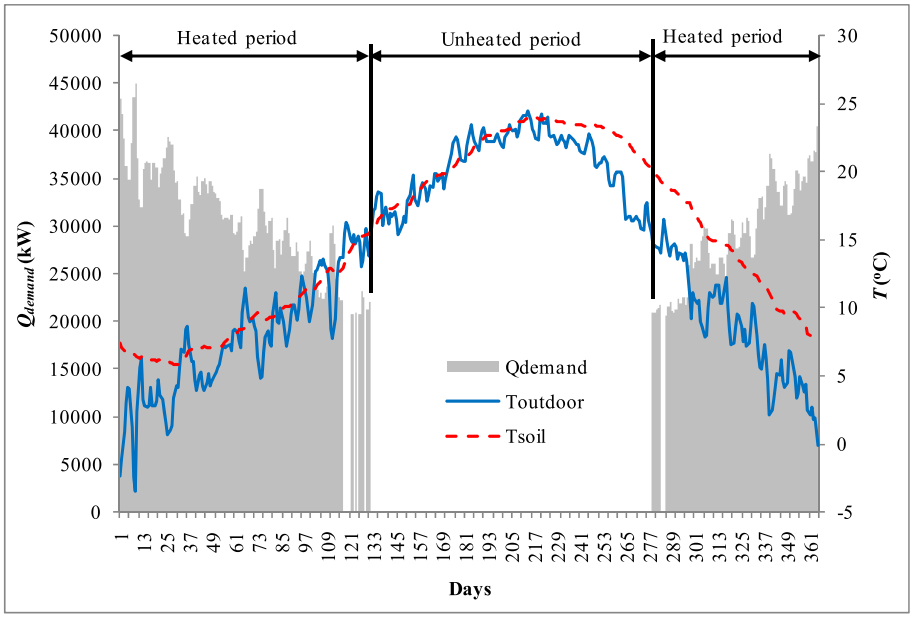

Fig. 3. Variation of outdoor temperature, soil temperature and heat demand of residences [13].

Table 1
Properties of PCM and working fluid used in HP system [32–35].

Properties	R600a	RT55	RT60	RT70HC
Boiling Point (C)	−11.7	–	–	–
Critical Temperature (C)	134.7	–	–	–
Critical Pressure (MPa)	3.63	–	–	–
Density, ρ (kg/m^3)	508.7*			
Liquid	–	770	770	770
Solid	–	880	880	880
Volumetric expansion, β	–	1.14	1.14	1.14
Latent heat capacity (kJ/kg)	–	140****	130****	230****
Conductive heat transfer coefficient, k (W/mK)	–	0.2	0.2	0.2
Dynamic viscosity, μ (Ns/m^2)	–	0.01	0.01	0.01
Specific heat, C_p (kJ/kgK)	2.67*	2	2	2
Melting temperature, $T_{melting}$ (C)	–	55	60	70
ODP	0**	–	–	–
GWP	~20***	–	–	–

*values at 56 °C, ** relative to R11, ***relative to CO_2, **** calculated according to Ref [33].

where h_i is the convective heat transfer coefficient for the pipe flow. This heat transfer mechanism is modelled as the boiling process. According to this, h_i includes two terms namely bubbling boiling heat transfer coefficient (h_b) and enforced convective coefficient (h_e). The calculation formula is given as follows [36]:

$$h_i = h_b + h_e \tag{5}$$

$$h_b = 0.0122\left(\frac{k_f^{0.79} C_{pf}^{0.45} \rho_f^{0.49}}{\sigma^{0.5} \mu_f^{0.29} h_{fg}^{0.24} \rho_g^{0.24}}\right) \Delta T_s^{0.24} \Delta P_s^{0.75} S \tag{6}$$

$$h_e = 0.023\left(\frac{G(1-x)D}{\mu_f}\right)^{0.8} Pr_f^{0.4} \frac{k_f}{D} F \tag{7}$$

where ΔT_s is the temperature difference between the inner surface temperature of the pipe (T_w) and the saturation temperature of the fluid (T_s). ΔP_s is the pressure difference between the pressure at the inner surface temperature of the pipe ($P_{s,\ Tw}$) and the saturation pressure of the fluid (P_s). σ, ρ, μ, x, C_p and k are the surface tension, density, dynamic viscosity, dryness fraction, specific heat and conductive heat transfer coefficient of the fluid, respectively. h_{fg} is the enthalpy of phase change. The subscripts f and g indicate the properties of the saturated liquid and saturated vapour, respectively. G is the mass velocity described as the mass flow rate for the unit cross-section area of the pipe ($G = 4\dot{m}/\pi D^2$). F and S are the enforced convection boiling factor and effectiveness factor, respectively. F is given by [36]:

$$\begin{aligned} F &= 1.0 && \tfrac{1}{X_t} \le 0.1 \\ F &= 2.35\left(\tfrac{1}{X_t} + 0.213\right)^{0.736} && \tfrac{1}{X_t} > 0.1 \end{aligned} \tag{8}$$

$$\begin{aligned} S &= \left(1 + 0.12 Re_{if}^{1.14}\right)^{-1} && Re_{if} \le 32.5 \\ S &= \left(1 + 0.42 Re_{if}^{0.78}\right)^{-1} && 32.5 < Re_{if} < 70 \\ S &= 0.1 && Re_{if} \ge 70 \end{aligned} \tag{9}$$

where X_t and Re_{if} are defined as the Martinelli parameter and two-phase Reynolds number, respectively. They are given as [36]:

$$X_t = \left(\frac{1-x}{x}\right)^{0.9} \left(\frac{\rho_f}{\rho_g}\right)^{0.5} \left(\frac{\mu_f}{\mu_g}\right)^{0.1} \tag{10}$$

$$Re_{if} = F^{1.25} \frac{G(1-x)D}{\mu_f} \tag{11}$$

According to this, the required pipe number is calculated as:

$$n_{pipe,discharging} = \frac{\dot{Q}_{design}}{\dot{Q}_{pipe,discharging}} \tag{12}$$

The heat losses from the TES unit were also taken into account in the modelling. Taking Fig. 1 into consideration, it is given as:

$$\dot{Q}_{TES,loss} = \frac{1}{\frac{1}{\frac{Nu_o \cdot k_o}{D}} + \frac{r_1}{k_4} ln\left(\frac{r_2}{r_1}\right) + \frac{r_1}{k_5} ln\left(\frac{r_3}{r_2}\right) + \frac{r_1}{k_6} ln\left(\frac{r_4}{r_3}\right) + \frac{r_4}{r_1} \frac{1}{h_{ambiance}}} A_{TES}(T_{TES} - T_{ambinece}) \tag{13}$$

where A_{TES} are the heat transfer coefficient and lateral area of the shell side of TES. T_{TES} is handled as the melting temperature of the PCM. $T_{ambiance}$ was taken as 10 °C for the substation as the non-heated space [31]. h_o is the convective heat transfer coefficient of the environment of the substation space, and the heat resistance value related to this value ($1/h_{ambiance}$) is taken as 0.17 m^{2}K/W [31]. Finally, the required volume of the TES system is calculated by taking the required PCM, charging pipes (n_1) and discharging pipes (n_2) volume was considered in the system volume. The total volume of the TES system is the sum of the pipe volume (V_{pipe}) and PCM volume (V_{PCM}). The related volume on daily basis is given by:

$$V_{TES} = \overbrace{\left(A_{pipe.}(n_1 + n_2) \cdot H\right)}^{V_{pipe}} + \overbrace{\left(\frac{86400 \cdot \left(\dot{Q}_{design} + \dot{Q}_{TES,loss}\right)}{Q_{TES}} \cdot \beta\right)}^{V_{PCM}} \tag{14}$$

where A_{pipe} is the cross-sectional area, H is the height of the TES system (1.5 m), β is the volumetric expansion rate of PCM during the phase change, and Q_{TES} is the latent heat capacity (see Table 1). The installed model was validated using the data from Wu et al. [38] and Mohaghegh et al. [39]. The results are in good agreement with the related references as given in the previous study by the authors [13].

The condenser (HE-2) side of the HP system was modelled as a shell-and-tube type heat exchanger in according to the common use. It was assumed that the refrigerant is circulating on the tube side. According to this, the average heat transfer coefficient for the condensation process is given by [36]:

$$h_{tube} = 0.555\left(\frac{g\rho_f\left(\rho_f - \rho_g\right)\left(h_{fg} + 0{,}375 C_{pf}(T_s - T_w) k_f^3\right)}{\mu_f (T_s - T_w) D}\right)^{0.25} \quad Re_g = \frac{\rho_g V_g D}{\mu_g} < 35000 \tag{15}$$

Here the wall temperature (T_w) is taken as the average of the inlet (T_6) and outlet (T_7) of HC. The inner diameter of the tubes was taken as 0.01 m. On the other hand, it was assumed that the heating circuit water is circulating in the shell side of the heat exchanger. The convective heat transfer coefficient is determined as [40,41]:

$$h_{shell} = \frac{\left(\overbrace{JRe_s Pr^{\frac{1}{3}}\left(\frac{\mu}{\mu_w}\right)^{0.14}}^{Nu}\right)k}{D_e} \tag{16}$$

where J is the dimensionless heat factor according to the Kern method and taken from Ref [40,42]. D_e is the equivalent shell diameter, and Re_s is the Reynolds number for the shell side. For the design of 30° triangle placement, these values are given as [41]:

$$D_e = \frac{4\left(\frac{\sqrt{3}P_t^2}{4}\right) - \frac{\pi D_o^2}{8}}{\frac{\pi D_o}{2}} \tag{17}$$

$$Re_s = \frac{\dot{m} D_e}{\mu(D_s - ND_0)D_s f} \tag{18}$$

where D_s is the inner diameter of the shell side (0.1445 m), D_o is the outer diameter of the tubes (0.017 m), N is the number of central tubes (7), P_t is the ratio of the distance between tube centres to D_o (1.25). f is baffle cut, which is defined as the ratio of baffle spacing (L_b) to D_o. f was kept in the range of 0.4 and 0.6 as advised in Ref. [42]. According to this the required heat transfer area of the condenser is given by:

$$A_{condenser} = \frac{\dot{Q}_{design}}{\left(\frac{1}{h_{tube}} + \frac{ln\left(\frac{D_o}{D_i}\right)}{k_{tube}} + \frac{1}{k_{ins}} ln\left(\frac{r_3}{r_2}\right) + \frac{D_o}{D_i}\frac{1}{h_{shell}}\right)\Delta T_{lm} F} \tag{19}$$

where k_{tube} is the conductive heat transfer coefficient of the tubes (Stainless steel-16.3 W/mK). ΔT_{lm} and F are the logarithmic mean temperature and correction factor [40,41]:

$$\Delta T_{lm} = \frac{(T_6 - T_b) - (T_7 - T_c)}{ln\left(\frac{T_6 - T_b}{T_7 - T_c}\right)} \tag{20}$$

$$F(R,P) = \frac{\sqrt{R^2+1}}{R-1} \frac{ln\left(\frac{1-P}{1-PR}\right)}{ln\left(\frac{2-P\left(R+1-\sqrt{R^2+1}\right)}{2-P\left(R+1+\sqrt{R^2+1}\right)}\right)} \tag{21}$$

where

$$R = \frac{T_6 - T_7}{T_b - T_c} and P = \frac{T_b - T_c}{T_b - T_7} \tag{22}$$

2.2. Modelling of heat exchangers for the heat centre and the heating circuit

A plate-type heat exchanger with titanium coating (HE-1) was used in the heat centre of GDHS to prevent the corrosion effects of the geothermal fluid. The efficiency of the exchanger was assumed as 0.98 to cope with the worst cases. The convective heat transfer coefficient for both hot and cold streams, the related heat transfer area and the number of required plates are given as [36]:

$$h = \left(\overbrace{0.2 \cdot Re^{0.67} \cdot Pr^{0.4} \cdot \left(\frac{\mu}{\mu_o}\right)^{0.1}}^{Nu}\right)\frac{k}{D_h} \tag{23}$$

$$A_{HE} = \frac{0.98\dot{m}_2(h_2 - h_3)}{\frac{1}{\frac{1}{h_i} + R_i + \frac{l}{k_{plate}} + R_o + \frac{1}{h_o}} \frac{(T_2 - T_4) - (T_3 - T_9)}{ln\left(\frac{T_2 - T_4}{T_3 - T_9}\right)}} \tag{24}$$

$$n_{plate} = \frac{A_{HE}}{A_{plate}} \tag{25}$$

where μ_o indicates the dynamic viscosity at the average temperature of the hot and cold streams. D_h is the hydraulic diameter (0.0139 m), *and* A_{plate} is the heat transfer area of a single plate (1.38 m^2) [43]. The aluminium panel radiator (HE-3) was used for the heating process of the residences in the heating circuit. The panel has a nominal height of 0.6 m. The required panel length was calculated taking the heat transfer ability into account for the peak heat demand of the residences. The heating capacity changes with the inlet (T_6) and outlet (T_7) temperatures of circulating water as given in Fig. 4 [44].

2.3. Heat losses of transmission lines

The heat loss per unit length in the pipelines is given by:

$$\dot{q}_{loss} = \frac{2\pi(T_i - T_o)}{\frac{1}{r_1 h_i} + \frac{1}{k_{pipe}} ln\left(\frac{r_2}{r_1}\right) + \frac{1}{k_{ins}} ln\left(\frac{r_3}{r_2}\right) + \frac{1}{k_{cover}} ln\left(\frac{r_4}{r_3}\right) + \frac{1}{k_{soil}} ln\left(\frac{r_5}{r_4}\right)} \tag{26}$$

where the convective heat transfer coefficient is defined by [36]:

$$h_i = \left(\overbrace{0.012\left(Re_D^{0.8} - 280\right)Pr^{0.4}}^{Nu}\right)\frac{k_{fluid}}{2r_i} \tag{27}$$

The used properties in Eq. (25) are given in Table 2. The diameter of the soil was determined the as the point where the heat losses can be neglected [6,44].

The temperature decrease depending on heat loss at the non-operational conditions is given by:

$$\Delta T = \frac{\dot{q}_{loss} \cdot L \cdot 86400}{mC_p} \tag{28}$$

2.4. The required power for pumps and compressor

The required power of the pumps is calculated in terms of pressure drops (ΔP). The required power of the compressor is calculated in terms of the designed conditions of HP as well as pressure drops. Assuming efficiency (η) of 0.8 for the pumps and compressor, the pump and compressor power are given by:

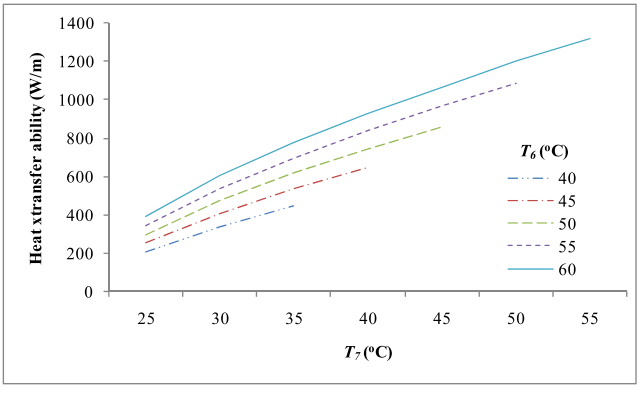

Fig. 4. The heating capacity of the aluminium panel radiator.

Table 2
Technical properties of the transmission lines [5,6].

Layer	Material	*k* (W/mK)	*r* (m) H-line	*T*-line	Length-*L* (m) H-line	*T*-line
Pipe	St-37 steel	76	0.20 (inner) 0.2063 (outer)	0.15 (inner) 0.1556 (outer)	4250	4000*
Insulation	polyurethane	0.028	0.28	0.23		
Cover	polyethylene	0.43	0.286	0.2352		
Soil	–	2.1	0.6			

*The longest line.

$$\dot{W}_{pump} = \frac{\dot{m} v \Delta P}{\eta} \tag{29}$$

$$\dot{W}_{compressor} = \frac{\dot{m}((h_b - h_a) + (v\Delta P))}{\eta} \tag{30}$$

The pressure drop is given as:

$$\Delta P = \lambda \frac{L}{D} \frac{\rho V^2}{2} \tag{31}$$

or for the shell side of the condenser (HE-2) unit [45];

$$\Delta P = 8 J_r \frac{D_G}{D_e} \frac{L}{L_b} \frac{\rho V^2}{2} \left(\frac{\mu}{\mu_w}\right)^{-0,14} \tag{32}$$

where L and D (or D_h) indicate the length of the pipes (or plates). λ denotes the friction factor and is given in terms of Reynolds number (Re). J_r is the dimensionless pressure factor according to the Kern method and taken from Ref [40,42], D_G is the nominal shell diameter (0.19 m). The used friction factors are given in Table 3.

3. Energy and exergy analysis

The general mass, energy, and exergy balances of *the* k^{th} component under steady-state conditions are given by:

$$\sum (\dot{m}_i)_k - \sum (\dot{m}_o)_k = 0 \tag{33}$$

$$\dot{Q}_k - \dot{W}_k + \sum (\dot{m}_i h_i)_k - \sum (\dot{m}_o h_o)_k = 0 \tag{34}$$

$$\left(1 - \frac{T_0}{T}\right)\dot{Q}_k - \dot{W}_k - \sum (\dot{m}_i \psi_i)_k - \sum (\dot{m}_o \psi_o)_k - \dot{E}x_{d,k} = 0 \tag{35}$$

where $\dot{Q}$ is the heat rate term, $\dot{W}$ is the work term, $\dot{m}$ is the mass flow rate. i indicates the inlet conditions, and o indicates the outlet conditions. Exergy of flow is given by:

$$\psi = (h - h_0) - T_0(s - s_0) \tag{36}$$

Here, h and s indicate orderly enthalpy and entropy at a particular state. Subscript 0 indicates the reference state conditions. The energy and exergy balance equations of the considered system are given in Table 4.

4. Economic and environmental evaluation

Net present Value (*NPV*) analysis is used for economic evaluation since it considers the time value of the cash flow for the lifetime of the handling systems [19,47]. *NPV* is given by:

$$NPV = \sum_{t=0}^{n} \frac{C_e + C_f - C_{o\&m}}{(1+r)^t} - (C_{TES} + C_{PCM} + C_{pr}) \tag{37}$$

where r, n, and t are the discount rate (15.75 %), the lifetime of the system (20 years) and the related year, respectively [48]. $C_{o\&m}$ is the operating and maintenance cost (10 % of the total investment cost) [49], C_e is the saved electricity cost (0.14 $/kWh) [50], C_f is the saved heating energy cost (12.92 $/MWh) [51]. C_{TES} is the investment cost of the TES unit, C_{PCM} is the investment cost of required PCM (95 $/ton) [52], $C_{HE\text{-}3}$ is the investment cost of the additional panel radiator (77.55 $/m) [53], $C_{compressor}$ is the investment cost of the compressor of HP system, $C_{HE\text{-}2}$ is the investment cost of the condenser of HP system, and C_{ev} is the investment cost of the expansion valve of HP system (26 $/residence) [54]. C_{TES} is calculated by [13]:

$$C_{TES} = 7.489 \cdot 10^{-7}(n_{pipe})^4 - 4.915 \cdot 10^{-4}(n_{pipe})^3 + 0.106(n_{pipe})^2 - 6.106 n_{pipe} + 741.040 \tag{38}$$

where n_{pipe} is the total number of charging and discharging pipes. $C_{compressor}$ is given by [55]:

$$C_{compressor} = -92.4\left(\dot{W}_{compressor}\right)^2 + 453.19\dot{W}_{compressor} + 28.01 \tag{39}$$

$C_{condenser}$ is given by [56]:

$$C_{condenser} = -58.82(A_{condenser})^2 - 487.34 A_{condenser} + 112.11 \tag{40}$$

In the environmental evaluation, prevented emissions by the save electricity and heat were considered. Since the required electricity of the region was supplied by a coal-fired power plant, the emission values related to the plant were considered. Since the

Table 3
The friction factors for the pumps and compressor.

Component	Friction Factor	Explanation	Source	
T-line pump (P_1)	Line side	*	–	[46]
	HE-1 side	$\lambda = \frac{1.22}{Re^{0.252}}$	–	[40]
H-line pump (P_2)	Line side	*	–	[46]
	HE-1 side	$\lambda = \frac{1.22}{Re^{0.252}}$	–	[40]
Substation pump (P_3)	TES side	$\lambda = \frac{64}{Re}$	$Re < 2300$	[40]
HC pump (P_4)	HE-3 side	$\lambda = \frac{15.064}{Re}$	–	[40]
Compressor	TES side	$\lambda = 0.316(\frac{1}{Re})^{0.25}$	$Re < 2{\cdot}10^4$	[36]
	HE-2 tube side	$\lambda = 0.184(\frac{1}{Re})^{0.20}$	$2{\cdot}10^4 < Re < 3 \cdot 10^5$	

*Taken from Moody diagram.

Table 4
Energy and exergy balance equations for TbHP-GDHS.

Components	Balance equation	Efficiency
T-line	$\dot{Q}_{T-line} = \dot{m}h_2 - \dot{m}h_1 - \dot{W}_{P1}$	$\eta = \frac{(\dot{m}h_2)}{\dot{m}h_1 + \dot{W}_{P1}}$
C	$\dot{Q}_C = (\dot{m}h_9 - \dot{m}h_4) - (\dot{m}h_3 - \dot{m}h_2)$	$\eta = \frac{(\dot{m}h_9 - \dot{m}h_4)}{(\dot{m}h_3 - \dot{m}h_3)}$
H-line	$\dot{Q}_{H-line} = (\dot{m}h_5 + \dot{m}h_9) - (\dot{m}h_4 + \dot{m}h_8) - \dot{W}_{P2}$	$\eta = \frac{(\dot{m}h_5 + \dot{m}h_9)}{(\dot{m}h_4 + \dot{m}h_8) + \dot{W}_{P2}}$
HP	$\dot{Q}_{HP} = (\dot{m}h_6 - \dot{m}h_7) - (\dot{m}h_5 - \dot{m}h_8) - \dot{W}_{P3} - \dot{W}_{compressor}$	$COP = \frac{(\dot{m}h_6 - \dot{m}h_7)}{\dot{W}_{compressor} + \dot{W}_{P3}}$
HC	$\dot{Q}_{useful} = \dot{m}h_7 - \dot{m}h_6 - \dot{W}_{P4}$	$\eta = \frac{\dot{Q}_{useful}}{(\dot{m}h_6 - \dot{m}h_7) + \dot{W}_{P4}}$
Overall system		$\eta = \frac{\dot{Q}_{useful}}{(\dot{m}h_1 - \dot{m}h_3) + \dot{W}_{total}}$
T-line	$\dot{E}x_{d,T-line} = (\dot{m}\psi_1 - \dot{m}\psi_2) + \dot{W}_{P1} - \left(1 - \frac{T_0}{T_{ave}}\right)\dot{Q}_{T-line}$	$\varepsilon = 1 - \frac{\dot{E}x_{d,T-line}}{\dot{m}\psi_1 + \dot{W}_{P1}}$
C	$\dot{E}x_{d,C} = (\dot{m}\psi_2 + \dot{m}\psi_9) - (\dot{m}\psi_3 + \dot{m}\psi_4) - \left(1 - \frac{T_0}{T_{ave}}\right)\dot{Q}_C$	$\varepsilon = 1 - \frac{\dot{E}x_{d,C}}{(\dot{m}\psi_2 - \dot{m}\psi_3)}$
H-line	$\dot{E}x_{d,H-line} = (\dot{m}\psi_4 + \dot{m}\psi_8) - (\dot{m}\psi_5 + \dot{m}\psi_9) + \dot{W}_{P2} - \left(1 - \frac{T_0}{T_{ave}}\right)\dot{Q}_{H-line}$	$\varepsilon = 1 - \frac{\dot{E}x_{d,H-line}}{(\dot{m}\psi_4 + \dot{m}\psi_8) + \dot{W}_{P2}}$
HP	$\dot{E}x_{d,HP} = (\dot{m}\psi_5 + \dot{m}\psi_7) - (\dot{m}\psi_8 + \dot{m}\psi_6) + \dot{W}_{P3} + \dot{W}_{compressor} - \left(1 - \frac{T_0}{T_{ave}}\right)\dot{Q}_{HP}$	$\varepsilon = 1 - \frac{\dot{E}x_{d,TbHP}}{(\dot{m}\psi_5 - \dot{m}\psi_8) + \dot{W}_{P3} + \dot{W}_{compressor}}$
HC	$\dot{E}x_{d,HC} = (\dot{m}\psi_6 - \dot{m}\psi_7) + \dot{W}_{P4} - \left(1 - \frac{T_0}{T_{ave}}\right)\dot{Q}_{useful}$	$\varepsilon = 1 - \frac{\dot{E}x_{d,HC}}{(\dot{m}\psi_6 - \dot{m}\psi_7) + \dot{W}_{P4}}$
Overall system	$\dot{E}x_{d,total} = \dot{E}x_{d,T-line} + \dot{E}x_{d,C} + \dot{E}x_{d,H-line} + \dot{E}x_{d,HP} + \dot{E}x_{d,HC}$	$\varepsilon = 1 - \frac{\dot{E}x_{d,total}}{(\dot{m}\psi_1 - \dot{m}\psi_3) + \dot{W}_{total}}$

most used energy source for heating is natural gas, the probable prevented emissions were considered taking handling the equivalent natural gas consumption. On the other hand, the emission prevented by saving heating energy was considered to be sourced from natural gas since it is the most used source in Turkey. The basis of the emissions is given in Table 5 [57–59].

5. Multi-Criteria decision making (MCDM) analysis

MCDM was successfully applied to the energy systems to determine the most efficient design [60]. Efficiency Analysis Technique with Output Satisficing (EATWOS) is a sufficient technique depending on the successful results for energy problems [13,61,62]. The efficiency value in EATWOS is given as [63]:

$$E_i = \frac{\sum_{j=1}^{J} v_j \cdot op_{ij}}{\sum_{k=1}^{K} w_k \cdot ip_{ik}} \tag{41}$$

where w_k and v_j are the weights of input and output parameters, respectively. ip_{ik} and op_{ik} are distance matrices for the input and output values, respectively. These values are given by:

$$ip_{ik} = 1 + s_{ik} - s_k^* \tag{42}$$

$$op_{ik} = 1 + r_{ij} - r_j^* \tag{43}$$

where s_{ik}, r_{ij}, s_k^* and $r_j^*$are normalized input, normalized output, maximum normalized input and maximum normalized output values, respectively. These values are given as follows:

$$s_{ik} = \frac{x_{ik}}{\sqrt{\sum_{i=1}^{K} x_{ik}^2}} \tag{44}$$

$$r_{ij} = \frac{y_{ij}}{\sqrt{\sum_{i=1}^{I} y_{ik}^2}} \tag{45}$$

$$s_k^* = \min_i \{s_k\} \tag{46}$$

$$r_j^* = \max_i \{r_j\} \tag{47}$$

The input (X) and output (Y) matrices in terms of the input (x) and output (y) values are respectively formed as follows:

$$\underline{X} = \begin{bmatrix} x_{11} & \cdots & x_{1K} \\ \vdots & \ddots & \vdots \\ x_{I1} & \cdots & x_{IK} \end{bmatrix} x_{ik} \in \mathbb{R}_{\geq 0} \quad \forall_i = 1, \cdots, I \quad \forall_k = 1, \cdots, K \tag{48}$$

$$\underline{Y} = \begin{bmatrix} y_{11} & \cdots & y_{1J} \\ \vdots & \ddots & \vdots \\ y_{I1} & \cdots & y_{IJ} \end{bmatrix} y_{ij} \in \mathbb{R}_{\geq 0} \quad \forall_i = 1, \cdots, I \quad \forall_j = 1, \cdots, J \tag{49}$$

Since the EATWOS aims for the maximum outputs with minimum inlets, the inlet parameters were modified to give the minimums. The inlet and outlet parameters are shown in Table 6.

Table 5
Basis of the emissions [57–59].

Source	Emission			
	CO_2	CO	NO_2	SO_2
Natural gas*	1.95023	0.00024	0.03384	–
Lignite**	0.47848	0.01418	0.00782	0.00077

*per kmole-fuel, **per kg-fuel.

6. Results and discussion

A new TbHP-GDHS was designed and parametrically analyzed from the thermodynamics, economics and environmental points of view. Different cases were formed considering the working conditions based on the temperature scales. Three temperature difference scales (ΔT_{min}) for the heat exchange process were handled in the development of the cases. In this way, ΔT_{min} was tried to be kept at 5 °C, 10 °C, and 15 °C as the minimum. ΔT_{min} for the main heat exchanger of C (HE-1) was kept at 5 °C since all the flows are at the liquid phase. In this range, the thermodynamically available designs were determined in a number 66 different cases. This means that the formed cases include the maximum and minimum available working conditions under the assumed minimum temperature difference. The formed cases are given in Table 7.

Under the circumstances of the designed systems, the energy analysis was conducted and energy balances were obtained to determine the characteristic parameters of the system. So, the heat

Table 6
The inlet and outlet parameters.

Inlet parameter	Modified outlet parameters	Outlet parameters
T_1	T_1	ε
T_3	1/ (T_1- T_3)	CO_2
T_5	1/ (T_5- T_8)	NPV
T_8	1/ T_8	
T_6	T_6	
T_7	1/(T_6- T_7)	
T_a	1/ (T_a- T_d)	
T_d		

losses (Q) and required power values (W) were obtained as given in Fig. 5.

According to Fig. 5, the heat losses range between 12,165.53 and 20,867.51 kW. The required compressor powers range between 3,357.61 and 13,029.91 kW. The required pump powers range between 5,544.57 and 13,647.65 kW. The main reason for the pump power and heat losses is the decrease in T_d and the increase in T_8. The compressor power is mainly affected by the variation of T_b. In light of energy analysis, the efficiency of GDHS

Table 7
The formed cases of TbHP-GDHS.

Cases	$T_{melting}$	T_1	T_2	T_3	T_4	T_5	T_6	T_7	T_8	T_9	T_a	T_b	T_c	T_d	$P_a = P_d$	$P_b = P_c$
ΔT$_{min}$ = 15 °C																
1	55	100	99.89	72.59	94.89	94.78	55	40	60	59.94	40	73.09	70	30	404.8	1087.5
2	55	100	99.89	72.59	94.89	94.80	55	40	65	64.94	40	73.09	70	30	404.8	1087.5
3	55	100	99.89	72.59	94.89	94.80	55	40	67	66.94	40	73.09	70	30	404.8	1087.5
4	55	100	99.89	73.76	94.89	94.80	55	40	67	66.94	40	81.07	70	20	302.2	1087.5
5	55	100	99.89	72.24	94.89	94.80	55	40	67	66.94	40	70.76	70	33	440.0	1087.5
6	60	100	99.89	72.00	94.89	94.80	55	40	67	66.94	40	70.76	70	33	440.0	1087.5
7	60	100	99.89	72.96	94.89	94.80	55	40	67	66.94	45	75.36	70	33	440.0	1087.5
8	60	100	99.89	71.73	94.89	94.80	55	40	66	65.94	45	73.81	70	35	464.8	1087.5
9	55	100	99.89	73.29	94.89	94.80	45	30	66	65.94	40	81.07	60	20	302.2	1087.5
10	55	100	99.89	70.87	94.89	94.80	45	30	65	64.94	40	61.02	45	20	302.2	604.5
11	60	100	99.89	70.62	94.89	94.80	45	30	65	64.94	40	61.02	45	20	302.2	604.5
12	60	100	99.89	71.17	94.89	94.80	45	30	65	64.94	40	65.06	50	20	302.2	684.9
13	60	100	99.89	70.62	94.89	94.80	45	30	65	64.94	40	60.85	50	25	350.7	684.9
14	60	100	99.89	70.51	94.89	94.80	45	30	65	64.94	40	60.01	50	26	361.0	684.9
15	60	100	99.89	70.84	94.89	94.80	45	30	65	64.94	40	62.54	50	23	330.6	684.9
16	60	100	99.89	70.85	94.89	94.80	45	30	65	64.94	40	62.75	45	18	284.8	604.5
17	60	100	99.89	71.07	94.89	94.80	45	30	65	64.94	40	64.47	45	16	267.2	604.5
18	60	100	99.89	71.17	94.89	94.80	45	30	65	64.94	40	64.91	55	25	350.7	773.0
19	60	100	99.89	70.94	94.89	94.80	45	30	65	64.94	40	63.26	55	27	371.6	773.0
20	60	100	99.89	70.61	94.89	94.80	45	30	65	64.94	40	60.79	55	30	404.7	773.0
21	60	100	99.89	71.17	94.89	94.80	45	30	65	64.94	40	64.89	60	30	404.7	869.2
22	60	100	99.89	71.11	94.89	94.80	55	45	65	64.94	45	70.44	60	29	393.5	869.2
23	60	100	99.89	72.29	94.89	94.80	60	45	65	64.94	45	77.71	70	30	404.7	1087.5
24	60	100	99.89	72.29	94.89	94.80	60	40	65	64.94	45	77.71	70	30	404.7	1087.5
25	70	110	109.87	80.93	104.87	104.78	60	40	75	74.93	55	75.26	55	30	404.7	773.0
26	70	110	109.87	81.46	104.87	104.78	60	40	75	74.93	55	79.20	60	30	404.7	869.2
27	70	110	109.87	82.01	104.87	104.78	60	40	75	74.93	55	83.13	65	30	404.7	973.9
28	70	110	109.87	81.46	104.87	104.78	60	40	75	74.93	55	79.38	55	25	350.7	773.0
29	55	95	94.89	67.21	89.89	89.81	55	40	60	59.95	40	70.63	67	30	404.7	1018.2
30	55	95	94.89	67.21	89.89	89.81	50	40	60	59.95	40	70.63	67	30	404.7	1018.2
31	55	95	94.89	66.51	89.89	89.81	50	40	60	59.95	40	65.71	61	30	404.7	889.4
32	55	95	94.89	65.84	89.89	89.81	45	35	60	59.95	40	60.79	55	30	404.7	773.0
33	55	100	99.89	70.86	94.89	94.79	45	35	60	59.94	40	60.79	55	30	404.7	773.0
34	55	110	109.87	80.94	104.87	104.73	45	35	60	59.92	40	60.79	55	30	404.7	773.0
ΔT$_{min}$ = 10 °C																
35	55	100	99.89	71.05	94.89	94.80	55	40	66	65.94	43	65.25	60	33	440.0	869.2
36	60	100	99.89	70.02	94.89	94.80	55	40	65	64.95	50	66.39	60	40	531.2	869.2
37	60	100	99.89	70.55	94.89	94.80	55	40	65	64.94	45	65.61	60	35	464.8	869.2
38	55	100	99.89	70.83	94.89	94.80	55	40	65	64.94	45	65.59	55	30	404.8	773.0
39	60	100	99.89	70.19	94.89	94.80	45	30	65	64.95	40	57.56	47	26	361.0	635.7
40	60	100	99.89	70.04	94.89	94.80	45	30	65	64.95	50	66.49	47	27	371.6	635.7
41	60	100	99.89	70.59	94.89	94.80	55	45	65	64.94	45	65.59	55	30	404.7	773.0
42	60	100	99.89	71.13	94.89	94.80	55	45	65	64.94	45	69.70	55	25	350.7	773.0
43	60	100	99.89	70.70	94.89	94.80	55	45	65	64.94	45	66.41	55	29	393.5	773.0
44	70	110	109.87	80.41	104.87	104.78	60	40	75	74.94	55	71.30	50	30	404.7	684.9
45	70	110	109.87	80.40	104.87	104.78	60	40	75	74.94	55	71.20	60	40	531.2	869.2
46	70	110	109.87	80.29	104.87	104.78	60	40	75	74.94	55	70.41	60	41	545.3	869.2
47	70	110	109.87	80.30	104.87	104.78	60	40	75	74.94	55	70.41	54	35	464.8	754.7
48	55	95	94.89	65.84	89.89	89.81	50	40	60	59.95	40	60.79	55	30	404.7	773.0
49	55	95	94.89	65.08	89.89	89.81	45	35	60	59.95	40	55.05	48	30	404.7	651.8
50	55	100	99.89	70.34	94.89	94.80	45	30	65	64.94	40	56.94	40	20	302.2	531.2
ΔT$_{min}$ = 5 °C																
51	55	100	99.89	69.73	94.89	94.79	55	45	60	59.94	50	62.32	55	40	531.2	773.0
52	60	100	99.89	70.02	94.89	94.80	60	50	65	64.95	50	66.39	60	40	531.2	869.2
53	60	100	99.89	70.55	94.89	94.80	60	50	65	64.94	45	65.61	60	35	464.8	869.2
54	60	100	99.89	70.05	94.89	94.80	55	45	65	64.95	45	61.55	50	30	404.7	684.9
55	70	110	109.87	80.40	104.87	104.78	65	55	75	74.94	55	71.20	60	40	531.2	869.2
56	70	110	109.87	80.29	104.87	104.78	65	55	75	74.94	55	70.41	60	41	545.3	869.2

(*continued on next page*)

Table 7 (*continued*)

ΔT_{min} = 15 °C Cases	$T_{melting}$	T_1	T_2	T_3	T_4	T_5	T_6	T_7	T_8	T_9	T_a	T_b	T_c	T_d	$P_a = P_d$	$P_b = P_c$
57	70	110	109.87	80.30	104.87	104.78	65	45	75	74.94	55	70.41	54	35	464.8	754.7
58	55	95	94.89	65.84	89.89	89.81	55	45	60	59.95	40	60.79	55	30	404.7	773.0
59	55	95	94.89	65.08	89.89	89.81	50	40	60	59.95	40	55.05	48	30	404.7	651.8
60	55	95	94.89	65.08	89.89	89.81	50	35	60	59.95	40	55.05	48	30	404.7	651.8
61	70	110	109.87	80.40	104.87	104.78	65	50	75	74.94	55	71.21	55	35	464.8	773.0
62	60	100	99.89	70.05	94.89	94.80	55	40	65	64.95	45	61.55	50	30	404.7	684.9
63	60	100	99.89	70.05	94.89	94.80	55	35	65	64.95	45	61.55	50	30	404.7	684.9
64	70	110	109.87	80.40	104.87	104.78	65	45	75	74.94	55	71.21	55	35	464.8	773.0
65	55	100	99.89	69.73	94.89	94.79	55	40	60	59.94	50	62.32	55	40	531.2	773.0
66	55	95	94.89	65.08	89.89	89.81	50	30	60	59.95	40	55.05	48	30	404.7	651.8

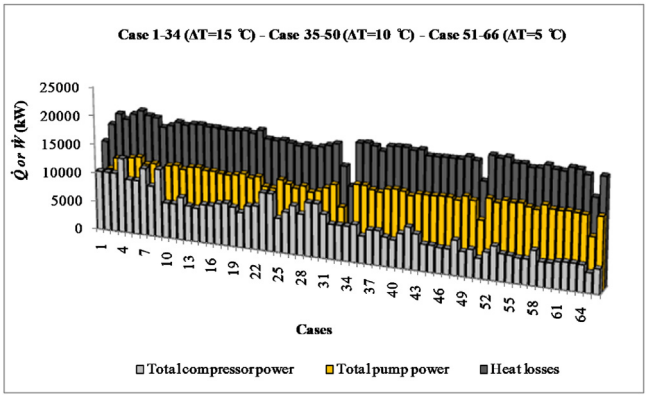

Fig. 5. Heat losses and power characteristics.

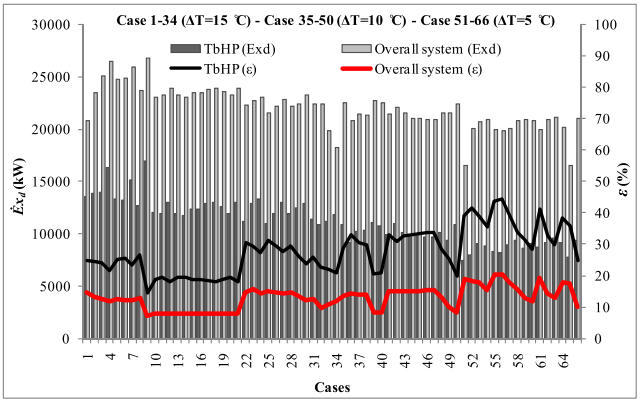

Fig. 7. The exergy analysis results.

and performance of the TbHP system were obtained as given in Fig. 6.

According to Fig. 6, the performance of TbHP ranges between 4.39 and 15.80, whereas the efficiency of the district heating system ranges between 72.90 % and 82.19 %. Contrary to expectations, the efficiency of the overall system does not increase with the increase in performance of the TbHP system. The main reason for this fact, depending on the attainable limits of the design, is the increase in the power requirement of pumps although the power requirement of TbHP decreases. From this point, the exergy analysis gives more clear view considering the quality of energy. The exergy results are given in Fig. 7.

According to Fig. 7, the exergy destruction ranges between 16,562.52 kW and 26,786.32 kW for the overall system. It ranges between 7,415.63 kW and 16,692.30 kW for the TbHP system. The main part of the exergy destruction depends on the conversion of the power consumption to lost heat energy. The exergy efficiency ranges between 7.15 % and 20.30 % for the overall system whereas it ranges between 14.39 % and 44.25 % for the TbHP system. The difference between the efficiency values is caused by the handled ΔT_{min} values. According to thermodynamic evaluation, the most effective case was determined as Case 56 from the exergy point of view and Case 34 from the energy point of view. Depending on the formed designs, one of the most important parameters is the saved energy for the economical and environmental evaluation as well as the performance criteria. The saved energy values for heat and electricity are given in Fig. 8.

According to Fig. 8, the electricity-sourced energy saving ranges between −10.13 GWh/year and 20.78 GWh/year whereas the heat-sourced saving ranges between 148.79 GWh/year and 196.30 GWh/year. The electricity saving is sourced by the equipment running on a design basis. So, some cases are not effective depending

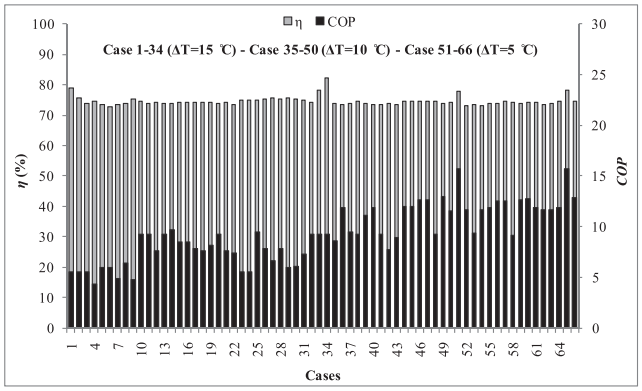

Fig. 6. Efficiency of the GDHS and performance of the TbHP system.

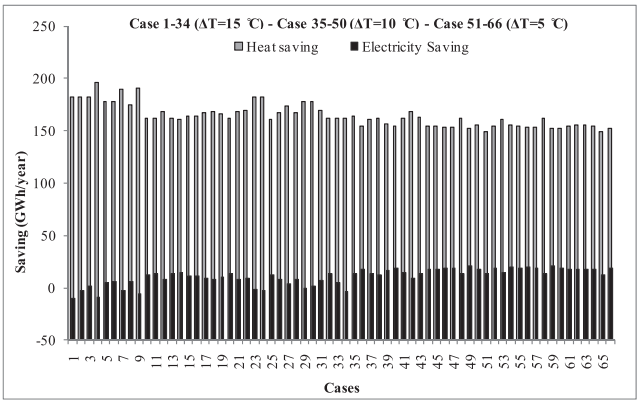

Fig. 8. Saving values of TES-based SGDHS.

on the designing parameters although the performance of TbHP is comparatively higher. The heat saving is sourced by the decrease in the use of geothermal fluid, which also directly affects the sustainability of the resources. For the economic evaluation of the newly designed system, the required heat transfer area of the condenser (HE-2) and the required volume of the evaporator (TES) are the most effective parameters. The variations of condenser area and TES volume are given in Fig. 9.

According to Fig. 9, the required condenser area ranges between 6,281.90 m^2 and 40,475.43 m^2. The TES volume ranges between 31,582.92 m^2 and 55,341.02 m^2. The condenser area is highly affected by ΔT_{min}. The required area increases with the decrease of ΔT_{min}. The required number of heating and cooling pipe has relatively lower effects on the volume of TES in comparison to the volume of PCM. So, the melting point of PCM is the most effective parameter on the required volume. Under these circumstances, the formed designs were evaluated from the economic point of view by the NPV method. The obtained results are given in Fig. 10.

According to Fig. 10, the largest part of the investment cost is sourced by the TbHP system. This cost varies between 20.98 million $ and 29.58 million $. The largest part of TbHP investment is sourced by TES unit which ranges between 44 % and 59 %. The condenser cost ranges between 20 % and 47 % whereas the compressor cost ranges between 6 % and 23 %. In the study, the additional panel radiator (HE-3) costs were also taken into account since the temperature scales of HC were handled as the designing parameter. This cost was not included in the calculations when the need was negative. Panel radiator costs reach up to 6.20 million $. According to this, the NPV values vary between −15.43 million $ and 6.35 million $. The electricity and heat saving are the incomes of the system. These values range between −1.42 million $ and

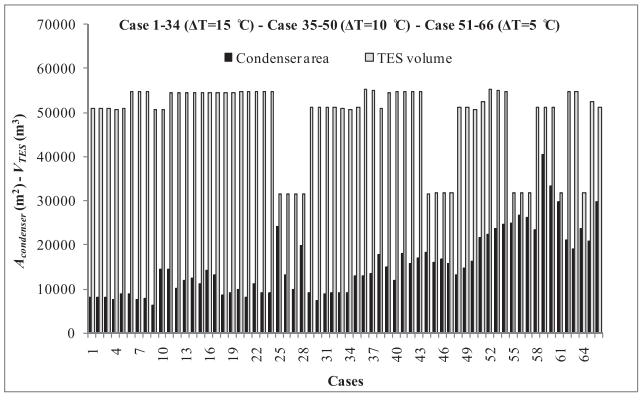

Fig. 9. Results of energy and exergy analyses.

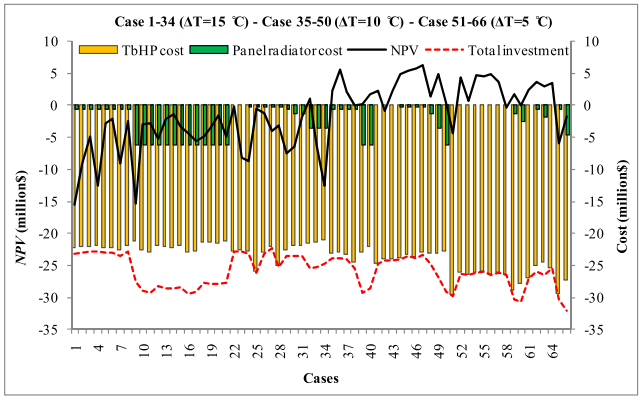

Fig. 10. Results of economic evaluation.

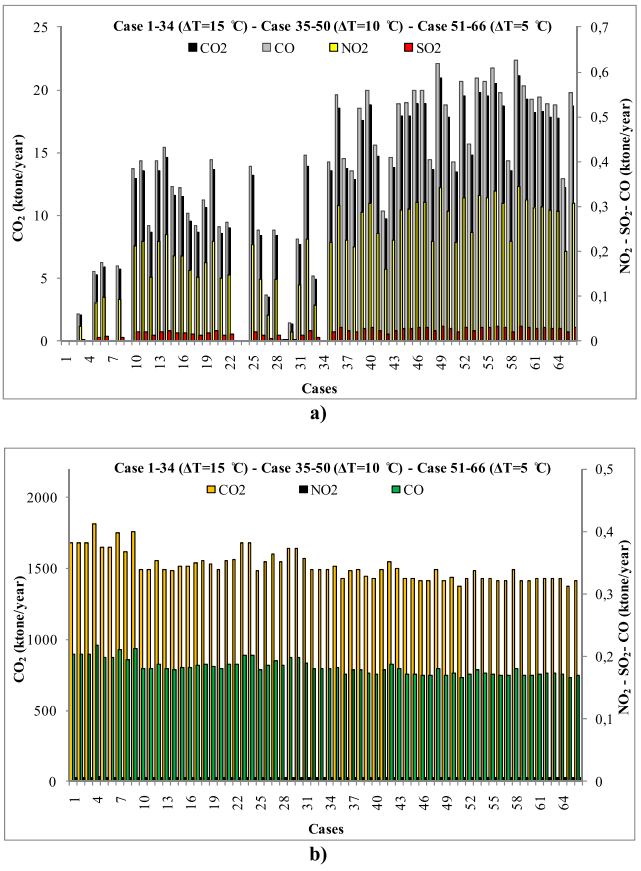

Fig. 11. Emission reduction sourced by electricity saving (a) and heat saving (b).

2.91 million $ for electricity savings whereas it ranges between 1.92 million $ and 2.54 million $ for heat savings. The most investable case was determined as Case 47 with the highest NPV value. The heat and electricity savings also directly affect emission reduction. The obtained results for the environmental evaluation are shown in Fig. 11.

According to Fig. 11, it is available to prevent the emission of CO_2 ranging between 1,384.87 ktones/year and 1,802.41 ktones/

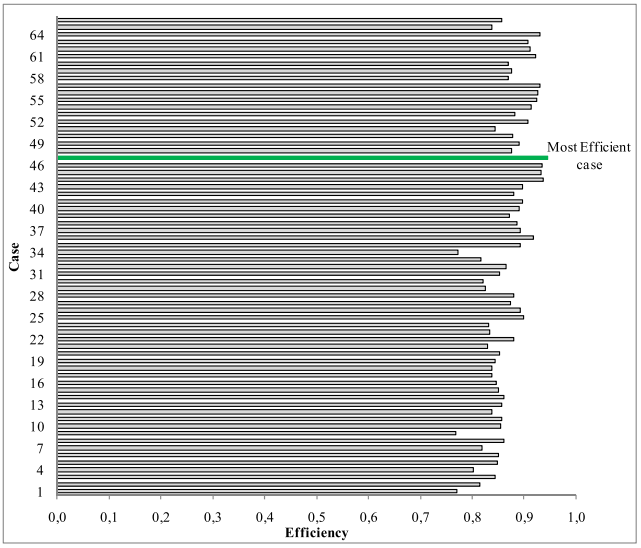

Fig. 12. EATWOS results and optimal solution.

year. The prevented emission of NO_2 ranges between 24.02 and 31.28 ktones/year. The prevented emissions of CO and SO_2 respectively reach up to 0.8 and 0.03 ktones/year. So, the most environment-friendly design was determined as Case 4.

Since the system includes many parameters which directly affect the results, it is very hard to make a decision on the optimum point. So, a multi-criteria decision-making analysis (EATWOS) was conducted to determine the most effective design. In the study, 7 input parameters and 3 output parameters were handled to make a decision point. Since it was thought that all the parameters have an equal significance, the weights were included in the analysis as 1/7 and 1/3 for the input and output parameters, respectively. The results of EATWOS are given in Fig. 12.

According to Fig. 12, the efficiency values change between 0.768 and 0.945. The most effective case was determined as Case 47. In this case, the exergy efficiency was calculated as 15.24 % with the highest NPV value of 6.35 million $. The CO_2 reduction was recorded as 1435.32 ktons/year. ΔT_{min} is 10 °C for this case whereas the melting temperature of PCM is 70 °C. The other design temperatures of T_1, T_3, T_6, T_7, T_8, T_a, T_b, T_c, and T_d were determined as 110 °C, 80.3 °C, 60 °C, 40 °C, 75 °C, 55 °C, T_b = 70.4 °C, 54 °C, and 35 °C, respectively. P_a and P_d are 464.77 kPa and 754.74 kPa, respectively.

The analyses with single output were also evaluated in the study. According to the results of these analyses, Case 61 was found the most efficient one from the exergy efficiency viewpoint

Table 8
Thermophysical characteristics of optimal TbHP-GDHS.

Points	Fluids	ṁ (kg/s)	T (°C)	P (kPa)	h (kJ/kg)	s (kJ/kgK)	v (m³/kg)	ψ(kJ/kg)	Ė(kW)	Ėx(kW)
0	H_2O	–	25.00	101.33	104.82	0.3674	–	–	–	–
	R600a				598.03	2.5104				
1	Geofluid	462.00	110.00		461.42	1.4188	0.001052	43.12	213,178.30	19,920.26
2	Geofluid	462.00	109.87		460.89	1.4174	0.001051	43.00	212,931.30	19,865.15
3	Geofluid	462.00	80.30		336.26	1.0792	0.001029	19.20	155,353.70	8,872.19
4	H_2O	447.87	104.87		439.75	1.3619	0.001047	38.39	196,949.46	17,194.47
5	H_2O	447.87	104.78		439.36	1.3609	0.001047	38.31	196,776.57	17,157.72
6	H_2O	671.04	60.00		251.19	0.8313	0.001017	8.04	168,556.68	5,398.42
7	H_2O	671.04	40.00		167.54	0.5723	0.001008	1.62	112,426.68	1,084.52
8	H_2O	447.87	75.00		314.03	1.0158	0.001026	15.86	140,644.27	7,104.49
9	H_2O	447.87	74.94		313.76	1.0151	0.001026	15.82	140,523.42	7,087.13
a	R600a	175.07	55.00	464.77	639.18	2.4359	0.091374	63.36	111,899.96	11,092.69
b	R600a	175.07	70.41	754.74	659.76	2.4359	0.056063	83.94	115,502.86	14,695.59
c	R600a	175.07	54.00	754.74	332.60	1.4384	0.001955	54.19	58,227.35	9,486.84
d	R600a	175.07	35.00	464.77	332.60	1.4449	0.013890	52.26	58,227.35	9,148.21

Table 9
Energy and exergy analysis results of optimal TbHP-GDHS.

Components	Ẇ(kW)	Q̇(kW)	Ė$_i$(kW)	Ė$_o$(kW)	Ėx$_i$(kW)	Ėx$_o$(kW)	Ėx$_d$(kW)	η (%)	ε (%)
T- line	1,533.29	−1,780.28	213,178.30	212,931.30	21,453.55	20,259.86	1,193.69	99.17	94.81
C		−1,151.55	57,577.60	56,426.05	10,992.95	10,319.91	673.04	98.00	93.88
H- line	11,203.76	−11,497.51	337,593.73	337,299.98	35,502.72	26,300.13	9,202.59	96.70	80.30
TbHP	4,532.43	−4,534.73	56,132.30	56,130.00	14,585.67	4,908.57	9,677.09	12.67*	33.65
HC	169.32	−56,299.32	168,556.68	112,426.68	5,398.42	1,084.52	127.71	99.70	97.71
Overall system	**17438.80**	**−19133.39**	**57,824.59**	**56,130.00**	**28,486.86**	**4,342.41**	**20,874.11**	**74.58**	**15.24**

*COP value.

Table 10
NPV analysis results of optimal TbHP-GDHS (in US$).

	Years					
	Present	**1**	**5**	**10**	**15**	**20**
Investment						
TES cost	−12,364,955.46					
Panel radiator addition cost	−199,543.06					
Paraffin	−123,705.82					
HP-compressor	−2,241,191.66					
HP-condenser	−7,894,402.10					
HP-expansion valve	−325,000.00					
Total	−23,148,798.10					
Cash flow						
Expenses						
Operating & Maintenance		61,824.78	61,824.78	61,824.78	61,824.78	61,824.78
Electricity benefit		2,602,350.13	2,602,350.13	2,602,350.13	2,602,350.13	2,602,350.13
Heat benefit		1,983,074.28	1,983,074.28	1,983,074.28	1,983,074.28	1,983,074.28
Salvage	2,314,879.81					
Total cash flow	−20,833,918.29	4,523,599.63	4,523,599.63	4,523,599.63	4,523,599.63	4,523,599.63
Cumulative cash flow	−20,833,918.29	−16,310,318.66	1,784,079.87	24,402,078.03	47,020,076.19	69,638,074.34
Discount rate (15,75 %)	1.000	0.864	0.481	0.232	0.111	0.054
Present value	−20,833,918.29	3,908,077.44	2,177,103.93	1,047,789.79	504,277.00	242,696.86
NPV	**6,346,416.74**					

of the system. In this case, the exergy efficiency was recorded as 19.19 % for T_1 = 110 °C and ΔT_{min} = 5 °C, whereas the CO_2 reduction and NPV were recorded as 1445.84 ktons/year and 2.49 million $. Case 4 was found the most efficient one from the CO_2 reduction point of view. In this case, the CO_2 reduction was recorded as 1680.73 ktons/year for T_1 = 100 °C and ΔT_{min} = 15 °C. The exergy efficiency was recorded as 11.94 % in this case. The NPV was recorded as % and −12.52 million $, which means it is not an investable design.

The thermophysical characteristics of Case 47 are given in Table 8. The energy and exergy analysis results obtained according to these characteristics are given in Table 9.

According to Table 9, the highest exergy destructions occur in the H-line and TbHP depending on the higher pump power requirement and heat losses. The exergy efficiency of the H-line was determined as 80.30 %. The exergy efficiency of the TbHP was determined as 33.65 % which is the lowest one due to higher heat losses and power requirements. The exergetic efficiency of the overall system was determined as 15.11 % whereas the energy efficiency was calculated as 74.58 %. The economic evaluation of Case 47 is given in Table 10.

According to Table 10, NPV is obtained equal to 6,346,416.74 $ which means an investable system. The system's payback period was determined as 4.5 years with a total investment cost of 23,148,798.1 $.

7. Conclusions

A new thermal energy storage-based geothermal district heating system (TbHP-GDHS) was designed and parametrically analyzed from the thermodynamics, economics and environmental points of view. The system includes a residential-type heat exchanger replaced with a substation heat exchanger. With this aim, a new heat pump system (TbHP) was designed including a TES unit as the evaporator and a condenser as the heat source of the heating circuit of the residences. 66 different cases were formed to investigate the new system considering different working parameters. The formed cases were analyzed from the thermodynamics, economics and environmental points. Finally, the cases were evaluated by the efficiency analysis technique with output satisficing (EATWOS) to make a decision for the optimal solution. The following findings were concluded:

- According to EATWOS results with 3 outputs, Case 47 was determined best case. In this case, the NPV is 6.35 million $. For this case, it was recorded a reduction of 1435.32 ktons in CO_2 emission per year, whereas the exergy efficiency of the system was recorded as 15.24 %.
- Case 47 is also the design with the highest NPV which means the parameter of NPV is the strongest one in the determination of the most efficient design.
- The new system is investable for lower ΔT_{min} values. When the lower ΔT_{min} values of 15 °C is taken into account, the required pump power decreases down to 5,544.57 kW whereas the saved heat reaches up to 196.30 GWh/year. It increases up to 13,648.65 kW for the lower ΔT_{min} values of 5 °C whereas the saved heat with 148.79 GWh/year is relatively lower. However, the required compressor power, depending on the thermodynamically limitations at the designing stage, the required compressor power increases up to 13,029.91 kW for the lower ΔT_{min} values of 15 °C whereas it decreases down to 3,557.61 kW for the lower ΔT_{min} values of 5 °C. Under this circumstances, the investment cost increase from 22.36 million $ to 32.08 million $. Although the higher ΔT_{min} values decrease the required heat transfer area and TES volume, it increases the power requirements. So, it is concluded that the highest NPV values are available for the temperature of 8–10 °C of ΔT_{min}.
- In comparison to current system, it available to save electricity consumption up to 20.78 GWh/year, and to save the used geothermal energy up to 196.30 GWh/year although extra power is required for the heat pump system. For the Case 47, the electricity and heat savings were recorded as 18.58 GWh/year and 153.53 GWh/year, respectively.
- In Case 47, the inlet temperature was recorded as 110 °C which is the highest one amongst all cases. This also means less power generation from a power plant integrated into GHDS. So, it should be evaluated in decision-making with its NPV value. The emission taxes also were not included in the analysis since there is no application in this way for Turkey. This criterion also should be evaluated in decision-making with its NPV value for a better decision.

Data availability

The data that has been used is confidential.

Declaration of Competing Interest

The authors declare that they have no known competing financial interests or personal relationships that could have appeared to influence the work reported in this paper.

References

[1] Lund JW, Huttrer GW., Toth AN. Characteristics and trends in geothermal development and use, 1995 to 2020. Geothermics 2022; 102522.
[2] O. Arslan, M.A. Ozgur, R. Kose, Electricity Generation Ability of the Simav Geothermal Field: A Technoeconomic Approach, Energy Sources, Part A: Recovery, Utilization, and Environmental Effects 34 (12) (2012) 1130–1144.
[3] A. Tugcu, O. Arslan, R. Kose, N. Yamankaradeniz, Thermodynamics and economical analysis of geothermal assisted absorption refrigeration system: Simav case study, J Turkish Soc Thermal Sci Technol 36 (2016) 143–159.
[4] J.W. Lund, A.N. Toth, Direct utilization of geothermal energy 2020 worldwide review, Geothermics 90 (2021) 101915.
[5] O. Arslan, R. Kose, Exergoeconomic optimization of integrated geothermal system in Simav, Kutahya. Energy Conversion and Management 51 (4) (2010) 663–676.
[6] O. Arslan, M.A. Ozgur, R. Kose, A. Tugcu, Exergoeconomic evaluation on the optimum heating circuit system of Simav geothermal district heating system, Energy and Buildings 41 (12) (2009) 1325–1333.
[7] O. Arslan, A.E. Arslan, Pareto principle-based advanced exergetic evaluation of geothermal district heating system: Simav case study, Journal of Building Engineering 58 (2022) 105035.
[8] L.F. Cabeza, V. Palomba, in: Encyclopedia of Energy Storage, Elsevier, 2022, pp. 338–350.
[9] B.R. Knudsen, D. Rohde, H. Kauko, Thermal energy storage sizing for industrial waste-heat utilization in district heating: A model predictive control approach, Energy 234 (2021) 121200.
[10] Y. Zhang, P. Johansson, A.S. Kalagasidis, Applicability of thermal energy storage in future low-temperature district heating systems – Case study using multi-scenario analysis, Energy Conversion and Management 244 (2021) 114518.
[11] E. Saloux, J.A. Candanedo, Model-based predictive control to minimize primary energy use in a solar district heating system with seasonal thermal energy storage, Applied Energy 291 (2021) 116840.
[12] H. Li, J. Hou, T. Hong, Y. Ding, N. Nord, Energy, economic, and environmental analysis of integration of thermal energy storage into district heating systems using waste heat from data centers, Energy 219 (2021).
[13] O. Arslan, A.E. Arslan, Performance evaluation and multi-criteria decision analysis of thermal energy storage integrated geothermal district heating system, Process Safety and Environmental Protection 167 (2022) 21–33.
[14] B. Rezaie, B.V. Reddy, M.A. Rosen, Exergy analysis of thermal energy storage in a district energy application, Renewable Energy 74 (2015) 848–854.
[15] H. Dorotić, T. Pukšec, N. Duić, Economical, environmental and exergetic multi-objective optimization of district heating systems on hourly level for a whole year, Applied Energy 251 (2019) 113394.
[16] Z. He, A.S. Farooq, W. Guo, P. Zhang, Optimization of the solar space heating system with thermal energy storage using data-driven approach, Renewable Energy 190 (2022) 764–777.
[17] D. Matuszewska, M. Kuta, P. Olczak, Techno-economic assessment of mobilized thermal energy storage system using geothermal source in Polish conditions, Energies 13 (2020) 3404.

[18] S.A. Kyriakis, P.L. Younger, Towards the increased utilization of geothermal energy in a district heating network through the use of a heat storage, Applied Thermal Engineering 94 (2016) 99–110.
[19] H. Arat, O. Arslan, Exergoeconomic analysis of district heating system boosted by the geothermal heat pump, Energy 119 (2017) 1159–1170.
[20] H. Arat, O. Arslan, Optimization of district heating system aided by geothermal heat pump: A novel multistage with multilevel ANN modelling, Applied Thermal Engineering 111 (2017) 608–623.
[21] Y. Wang, Y. Zhang, Analysis of the dilatancy technology of district heating system with high-temperature heat pump, Energy and Buildings 47 (2012) 230–236.
[22] Q. Zhang, M. Cao, Q. Zhang, H. Di, Research on a new district heating method combined with hot water driven ground source absorption heat pump, Energy Procedia 75 (2015) 1242–1248.
[23] R. Marx, D. Bauer, H. Drueck, Energy efficient integration of heat pumps into solar district heating systems with seasonal thermal energy storage, Energy Procedia 57 (2014) 2706–2715.
[24] S. Kang, H. Li, J. Lei, L. Liu, B. Cai, G. Zhang, A new utilization approach of the waste heat with mid-low temperature in the combined heating and power system integrating heat pump, Applied Energy 160 (2015) 185–193.
[25] B. Bach, J. Werling, T. Ommen, M. Münster, J.M. Morales, B. Elmegaard, Integration of large-scale heat pumps in the district heating systems of Greater Copenhagen, Energy 107 (2016) 321–334.
[26] D. Kim, D. Lee, J. Heo, M. Kim, Empirical results and operational cost analysis of geothermal heat pump system using thermal energy storage in cooling season, Korean Journal of Air-Conditioning and Refrigeration Engineering 30 (4) (2018) 167–174.
[27] H. Hemmatabady, B. Welsch, J. Formhals, I. Sass, AI-based enviro-economic optimization of solar-coupled and standalone geothermal systems for heating and cooling, Applied Energy 311 (2022) 118652.
[28] S. Siddiqui, J. Macadam, M. Barrett, The operation of district heating with heat pumps and thermal energy storage in a zero-emission scenario, Energy Reports 7 (2021) 176–183.
[29] M. Fiorentini, P. Heer, L. Baldini, Design optimization of a district heating and cooling system with a borehole seasonal thermal energy storage, Energy 262 (2023) 125464.
[30] S. Bordignon, D. Quaggiotto, J. Vivian, G. Emmi, G. De Carli, A. Zarrella A., A solar-assisted low-temperature district heating and cooling network coupled with a ground-source heat pump, Energy Conversion and Management 267 (2022).
[31] TSE (Turkish Standards Institution). TS 825: Thermal insulation requirements for buildings; May 2008.
[32] Refprop, Reference Fluid Thermodynamics and Transport Properties. NIST Reference Database. Version 9.0. National Institute of Standards, and Technology, NIST, USA, 2010.
[33] RUBITHERM. Phase change materials. Available from: https://www.rubitherm.eu/en/index.php/ productcategory /organische-pcm-rt. Last access: April 7th, 2022.
[34] M. Tenpierik, Y. Wattez, M. Turrin, T. Cosmatu, S. Tsafou, Temperature Control in (Translucent) Phase Change Materials Applied in Facades: A Numerical Study, Energies 12 (2019) 3286.
[35] S. Devotta, A.S. Padalkar, N.K. Sane, Performance assessment of HC-290 as a drop-in substitute to HCFC-22 in a window air conditioner, Int. J. Refrigeration 28 (4) (2005) 594–604.
[36] H. Yuncu, S. Kakac, Basic Heat transfer, Bilim Publishing, Ankara, 1999, in Turkish.
[37] J.S. Lim, A. Bejan, The Prandtl number effect on melting dominated by natural convection, ASME Journal Heat Transfer 114 (1992) 784–787.
[38] Y. Wu, D. Li, W. Jiang, S. Zhu, X. Zhao, M. Arici, E. Tuncbilek, Energy storage and exergy efficiency of a shell and tube latent thermal energy storage unit with non-uniform length and distributed fins, Sustainable Energy Technologies and Assessments 53 (2022).
[39] M.R. Mohaghegh, S.H. Tasnim, S. Mahmud, A geometrical optimization and comparison study on the charging and discharging performance of shell-and-tube thermal energy storage systems, Journal of Energy Storage 51 (2022) 104549.
[40] O.F. Genceli, Heat exchangers, Birsen Publication, Istanbul, 1999, in Turkish.
[41] S. Kakac, H. Liu, A. Pramuanjaroenkij, Heat Exchangers Selection, Rating and Thermal Design, 3th edition., CRC Press, Taylor and Francis Group, Florida, 2012.
[42] O. Kizilkan, Investigation of the effects of the baffles on the heat transfer coefficient and pressure drop in a shell and tube heat exchanger, Suleyman Demirel University Journal of Natural and Applied Sciences 11 (2009) 246–251.
[43] Jiangyin M&C Heat Parts, 2022. NT250L type heat exchangers. Available from: https://turkish.heat-exchangergasket.com/sale-14362173-titanium-0-5mm-nt250l-plate-heat-exchanger-plate-for-sea-water-fluid.html. Last access: October 15th, 2022.
[44] O. Arslan, Ultimate evaluation of Simav-Eynal geothermal resources: design of integrated system and its energy-exergy analysis, Eskisehir Osmangazi University, Institute of Applied Sciences, 2008, PhD Thesis.
[45] R. Selbaş, Ö. Kızılkan, M. Reppich, A new design approach for shell-and-tube heat exchangers using genetic algorithms from economic point of view, Chemical Engineering and Processing 45 (4) (2006) 268–275.
[46] Y.A. Cengel, J.M. Boles, Fluid mechanics: Fundamentals and Applications, 4th edition., McGraw Hill, New York, 2018.
[47] A. Akbulut, O. Arslan, H. Arat, O. Erbaş, Important aspects for the planning of biogas energy plants: Malatya case study, Case Studies in Thermal Engineering 26 (2021) 101076.
[48] CBRT (Central Bank of the Republic of Turkey). 2022. Inflation report, Available from: https://www.tcmb.gov.tr/wps/wcm/connect/EN/TCMB+EN/Main+Menu/Core+Functions/Monetary+Policy/Rediscount+and+Advance+Interest+Rates. Last Access: June 7th, 2022.
[49] O. Arslan, D. Kilic, Concurrent optimization and 4E analysis of organic Rankine cycle power plant driven by parabolic trough collector for low-solar radiation zone, Sustainable Energy Technologies and Assessments 46 (2021) 101230.
[50] EPDK (Energy Market Regulatory Authority of Rebuplic of Turkey). 2022. Electricity tariffs. Available from: https://www.epdk.gov.tr/Detay/Icerik/3-1327/elektrik-faturalarina-esas-tarife-tablolari. Last Access: June 7th, 2022.
[51] Iz-Geo (Izmir Geothermal A.Ş). 2022. Heating tariffs. Available from: https://www.izmirjeotermal.com.tr/islemler-ucret-tarifeleri-2021-2022-isitma-sezonu. Last Access: June 7th, 2022.
[52] Indiamart. 2022. The price of paraffin wax. Available from: https://www.indiamart.com/proddetail/chlorinated-paraffin-wax-22420468491.html. Last Access: June 7th, 2022.
[53] Demirdokum. 2022. PKKP 600 type panel radiator. Available from: https://www.cimri.com/radyator/en-ucuz-demirdokum-pkkp-600-1000-panel-plus-radyator-fiyatlari, 503553. Last Access: June 7th, 2022.
[54] Danfos. 2022. The price of the expansion valve. Available from: https://dir.indiamart.com/impcat/expansion-valve.html. Last Access: June 7th, 2022.
[55] Tecumseh Europe. 2022. The price of refrigerant compressors. Available from: https://www.yelkensogutma.com.tr/tr/9-kompresoerler. Last Access: June 7th, 2022.
[56] MIT heat exchangers. 2022. The price of shell and tube type heat exchangers. Available from: https://www.ekinmarket.com/borulu-isi-esanjorleri?sort=p.price&order=ASC. Last Access: June 7th.
[57] O. Arslan, E. Acikkalp, G. Genc, A multi-generation system for hydrogen production through the high-temperature solid oxide electrolyzer integrated to 150 MW coal-fired steam boiler, Fuel 315 (2022) 123201.
[58] O. Arslan, O. Erbas, Investigation on the improvement of the combustion process through hybrid dewatering and air pre-heating process: A case study for a 150 MW coal-fired boiler, Journal of the Taiwan Institute of Chemical Engineers 121 (2021) 229–240.
[59] O. Arslan, M.A. Ozgur, H.D. Yildizay, R. Kose, Fuel Effects on Optimum Insulation Thickness: An Exergetic Approach, Energy Sources Part A 32 (2009) 128–147.
[60] A.E. Arslan, O. Arslan, S.Y. Kandemir, AHP–TOPSIS hybrid decision-making analysis: Simav integrated system case study, Journal of Thermal Analysis and Calorimetry 145 (3) (2021) 1191–1202.
[61] A.E. Arslan, M.S. Acar, O. Arslan, Optimization of O-type ORC-Binary geothermal power plant: EATWOS analysis, BSEU Journal of Science 6 (2019) 222–236, https://doi.org/10.35193/bseufbd.601745.
[62] O. Arslan, A.E. Arslan, M.S. Acar, Multi-Criteria Making-Decision Modeling of b-type ORC-Binary Geothermal Power Plant: EATWOS Analysis, BSEU Journal of Science 6 (2019) 29–48, https://doi.org/10.35193/bseufbd.561668.
[63] M.L. Peters, S. Zelewski, Efficiency Analysis under Consideration of Satisficing Levels for Output Quantities, In Proceedings of the 17th Annual Conference of the Production and Operations Management Society (POMS), April 28-May 01, 2006, Boston, USA.